remote sensing

MDPI

Article

Three-Dimensional Structure and Transport Properties of Dust Aerosols in Central Asia—New Insights from CALIOP Observations, 2007–2022

Jinglong Li [1,2], Qing He [3,4,5,6,7,*], Yonghui Wang [1,2], Xiaofei Ma [8,9], Xueqi Zhang [8,9] and Yongkang Li [10]

1 College of Geographic Science and Tourism, Xinjiang Normal University, Urumqi 830054, China; jinglongli3s@xjnu.edu.cn (J.L.); wyhsd_3011@xjnu.edu.cn (Y.W.)
2 Xinjiang Laboratory of Lake Environment and Resources in Arid Zone, Urumqi 830054, China
3 Institute of Desert Meteorology, China Meteorological Administration, Urumqi 830002, China
4 National Observation and Research Station of Desert Meteorology, Taklimakan Desert of Xinjiang, Urumqi 830002, China
5 Taklimakan Desert Meteorology Field Experiment Station of China Meteorological Administration, Urumqi 830002, China
6 Xinjiang Key Laboratory of Desert Meteorology and Sandstorm, Urumqi 830002, China
7 Key Laboratory of Tree-Ring Physical and Chemical Research, China Meteorological Administration, Urumqi 830002, China
8 State Key Laboratory of Desert and Oasis Ecology, Key Laboratory of Ecological Safety and Sustainable Development in Arid Lands, Xinjiang Institute of Ecology and Geography, Chinese Academy of Sciences, Urumqi 830011, China; mxf@ms.xjb.ac.cn (X.M.); zhangxueqi@ms.xjb.ac.cn (X.Z.)
9 Research Centre for Ecology and Environment of CA, Chinese Academy of Sciences, Urumqi 830011, China
10 College of Geography and Remote Sensing Sciences, Xinjiang University, Urumqi 830017, China; yongkangl@stu.xju.edu.cn
* Correspondence: qinghe@idm.cn

Abstract: Central Asia (CA) is one of the major sources of global dust aerosols. They pose a serious threat to regional climate change and environmental health and also make a significant contribution to the global dust load. However, there is still a gap in our understanding of dust transport in this region. Therefore, this study utilizes Cloud–Aerosol LiDAR with Orthogonal Polarization (CALIOP) data from 2007 to 2022 to depict the three-dimensional spatiotemporal distribution of dust aerosols over CA and to analyze their transport processes. In addition, the Tropospheric Monitoring Instrument (TROPOMI) was employed to assist in monitoring the movement of typical dust events, and the trajectory model was utilized to simulate the forward and backward trajectories of a dust incident. Additionally, a random forest (RF) model was employed to rank the contributions of various environmental factors. The findings demonstrate that high extinction values (0.6 km^{-1}) are mostly concentrated within the Tarim Basin of Xinjiang, China, maintaining high values up to 2 km in altitude, with a noticeable decrease as the altitude increases. The frequency of dust occurrences is especially pronounced in the spring and summer seasons, with dust frequencies in the Tarim Basin and the Karakum and Kyzylkum deserts exceeding 80%, indicating significant seasonal and regional differences. The high values of dust optical depth (DOD) in CA are primarily concentrated in the summer, concurrent with the presence of a stable aerosol layer of dust in the atmosphere with a thickness of 0.62 km. Furthermore, dust from CA can traverse the Tianshan mountains via the westerlies, transporting it eastward. Additionally, skin temperature can mitigate regional air pollution. Our results contribute to a deeper understanding of the dynamic processes of dust in CA and provide scientific support for the development of regional climate regulation strategies.

Keywords: dust aerosols; central Asia; three-dimensional distribution; CALIPSO; spatiotemporal variation

Citation: Li, J.; He, Q.; Wang, Y.; Ma, X.; Zhang, X.; Li, Y. Three-Dimensional Structure and Transport Properties of Dust Aerosols in Central Asia—New Insights from CALIOP Observations, 2007–2022. *Remote Sens.* **2024**, *16*, 2049. https://doi.org/10.3390/rs16122049

Academic Editors: Alexander Kokhanovsky and Dmitry Efremenko

Received: 6 May 2024
Revised: 1 June 2024
Accepted: 3 June 2024
Published: 7 June 2024

1. Introduction

The rapid pace of industrial development coupled with the ongoing expansion of urban areas has increasingly highlighted air pollution concerns among the public, eliciting heightened scrutiny and concern for environmental issues, especially those tied to aerosols [1–3]. Aerosol particles, as key constituents of the Earth's atmosphere, are central to understanding changes in global and regional climates, environments, ecosystems, and the radiative equilibrium within the Earth–atmosphere interface [4–7]. These particles directly influence the Earth–atmosphere energy budget by absorbing and scattering sunlight and indirectly affect the climate by serving as nuclei for cloud condensation and ice formation, which modifies the properties, formation, and duration of clouds, thus impacting radiation dynamics and precipitation patterns [8–11]. Furthermore, these aerosols can heat the atmosphere by re-emitting absorbed solar energy as thermal radiation, leading to potential evaporation of cloud droplets. This process reduces cloud reflectivity, thereby exerting an influence on the climate known as the semi-direct climate effect [12–14].

Representing the most prevalent form of aerosols within the atmosphere, dust aerosols contribute to over half of the aerosol mass on a global scale [15]. Studies indicate that three-quarters of these aerosols stem from natural sources [16]. Undergoing continuous transformations through physical and chemical processes, dust aerosols intricately involve themselves in cloud formation and directly influence the Earth's radiation balance, thereby playing a critical role in the dynamics of the global climate [17,18]. Positioned within the semi-arid and arid zones of mid-latitude continents, CA is highly susceptible to climate variability, posing significant risks to water security and ecosystem stability on a global scale [19]. The region is now under scrutiny for its dust pollution challenges, which interface with both natural ecosystems and socio-economic frameworks, prompting investigations into the feedback mechanisms at play [20–22]. This area features a diverse aerosol composition, ranging from Middle Eastern mineral dust to desert dust emanating from the Tarim Basin, and even includes aerosols generated by lake desiccation [23]. These particles are propelled from the Earth's surface to the upper troposphere, facilitating their transport over considerable distances [24]. Furthermore, the sparse vegetation cover and enduring scarcity of water, combined with frequent dust events, earmark CA as a primary source of dust emissions, contributing 17–20% to the global tally [25]. Recent analyses have highlighted the dominance of severe dust storms in shaping the regional climate of CA, adversely affecting agricultural yield and human well-being, while the transregional movement of dust poses threats to ecosystems far beyond the local area [26]. In the context of escalating desertification, the release of dust is also altering water resource allocation and availability in a critical manner [27,28]. Despite these significant impacts, research focusing on the three-dimensional patterns and transport behaviors of dust aerosols specific to CA is lacking. At the same time, our understanding of the dust source regions and emissions in CA still has considerable gaps. Thus, precisely determining the vertical optical properties of dust aerosols, coupled with a detailed multi-perspective analysis of diverse data sources, is crucial for an in-depth understanding of the dust distribution and movement mechanisms covering CA's arid landscapes and their origins.

The advancement in satellite remote sensing technology, characterized by its high-resolution capabilities and extensive data coverage, has markedly enhanced its applicability in the realm of scientific inquiries [29,30]. Notably, the examination of aerosol vertical structures has benefitted from improved observation instruments. The CALIOP lidar system, deployed on the CALIPSO satellite, significantly facilitates the study of vertical dust aerosol patterns and movements. Its provision for the continuous, all-condition surveillance of both clouds and aerosols plays a crucial role in the precise assessment of dust aerosol distribution within CA. It should be highlighted that, in recent times, key global dust sources like the Taklimakan Desert and the Sahara Desert have been the focus of detailed studies leveraging CALIOP lidar technology [31–34]. CALIOP's adeptness at delineating the three-dimensional aspects and movement traits of dust aerosols, owing to its capability to discern between various aerosol types, is particularly noted [35]. Hence, there

is an ongoing need to enhance the construction and examination of the three-dimensional distribution and movement particularities of dust aerosols across the dry expanses of CA over extended timeframes and vast geographic expanses. This effort aims to elucidate variations in dust aerosols' optical characteristics, thus enriching our comprehension of their distribution and movement within this specific geographical locale.

Given this context, the present study aims to enhance the current understanding of dust aerosols in CA by (1) utilizing data from the CALIPSO satellite spanning 2007–2022 to construct a three-dimensional structure of dust optical parameters across the region and analyzing the frequency of dust aerosol occurrences across different altitude gradients; (2) calculating multi-year monthly and seasonal averages of DOD values and revealing the characteristics of the dust layer over the study area; (3) employing the Hybrid Single-Particle Lagrangian Integrated Trajectory (HYSPLIT) model to diagnose and analyze typical dust weather processes; (4) assessing the degree of contribution of multiple environmental covariates to dust aerosols over CA; and (5) examining the characteristics of aerosols across the entire CA region. These efforts are anticipated to significantly refine our comprehension of dust aerosols within CA.

2. Data and Methods

2.1. Study Area

Primarily situated between latitudes 35°N and 55°N and longitudes 46°E and 97°E, the arid zone of CA is highlighted in Figure 1 as a pivotal segment of the Silk Road Economic Belt, playing a crucial role in the emission of dust globally [36]. This zone includes the territories of Kazakhstan, Uzbekistan, Turkmenistan, Kyrgyzstan, Tajikistan, and the Xinjiang region in China [37]. Its landscape is characterized by a gradient from higher elevations in the southeast to lower ones in the northwest, encompassing deserts, plains, and mountain ranges [38]. The climate of this vast area is mainly of a dry continental nature, marked by intense solar radiation and high rates of evaporation [39]. These conditions, combined with widespread land degradation and the acute erosion of soil and water, have transformed CA's arid region into a significant zone of desertification on a global level [40]. This ongoing intensification of desertification not only exacerbates serious dust issues but also enhances the worldwide circulation of dust [25].

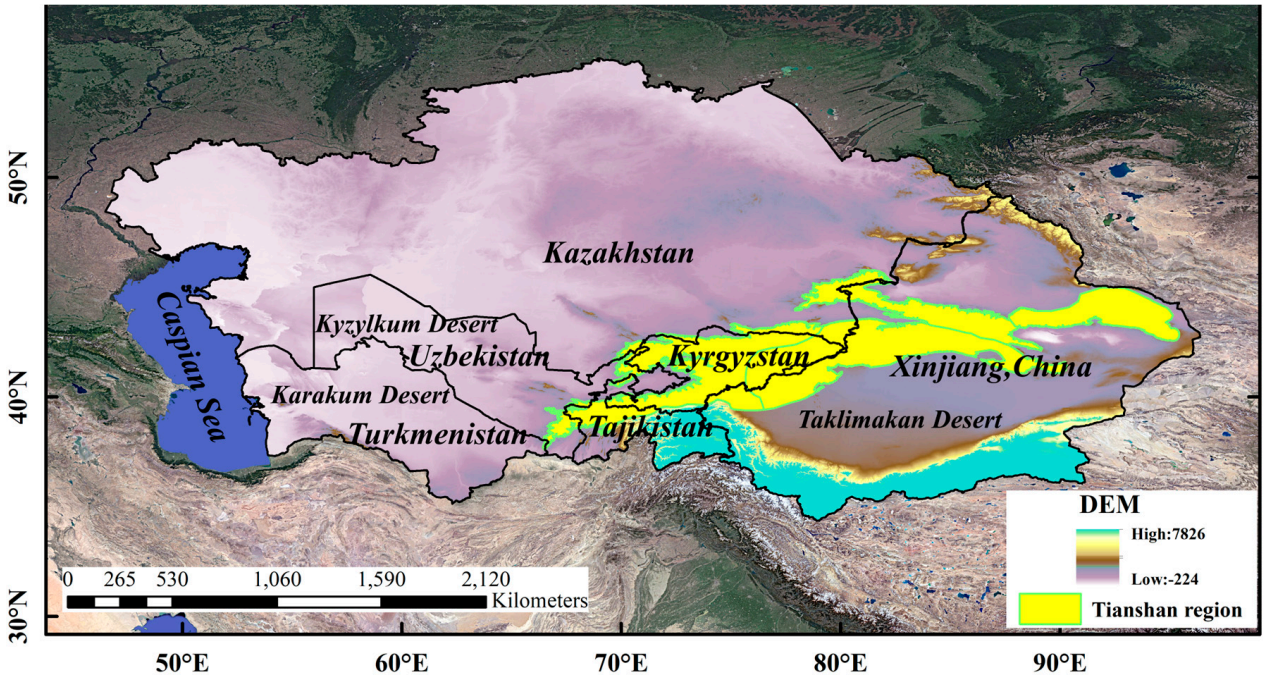

Figure 1. Overview of the study area.

2.2. CALIPSO Data

Initiated on 28 April 2006, the collaborative venture between NASA and CNES brought the CALIPSO satellite into orbit, featuring the CALIOP lidar as a critical instrument. This satellite is integrated into the A-Train satellite constellation, which operates in orbit at a height of 705 km above the Earth, maintaining an orbital inclination of 98 degrees. Leading this orbital assembly, the Aqua satellite makes its equatorial crossings around 13:30 and 01:30 local time, adhering to a 16-day orbit repetition schedule. It is noted that daytime measurements may suffer from sunlight dispersion, which can obscure the collected data by increasing the background noise. On the flip side, nighttime observations are prized for their higher signal-to-noise ratio, which translates to more distinct and reliable data. Therefore, this research predominantly utilizes nighttime data collections. It is important to recognize the data structure of CALIPSO: its Level 1 data presentations are refined to a horizontal resolution of 333 m, whereas its Level 2 data, spanning the vertical expanses from -0.5 to 20.2 km and further up to 30.1 km, are characterized by a horizontal resolution of 5 km and vertical resolutions of 60 m and 120 m at the respective intervals. With these technological advantages in hand, our investigation endeavors to (1) Employ the Level 2 Vertical Feature Mask (VFM) for detailed insights into dust occurrence, scrutinizing the dust layers' distribution (top, base, and thickness) and their frequency over the examined locale. (2) Investigate the spatial arrangement and optical characteristics (including the extinction coefficient and backscatter coefficients, along with the depolarization ratio) of dust aerosols, utilizing the Aerosol Profile (APRO) Level 2 product. (3) Calculate the aerosols' optical depth by vertically integrating extinction coefficients, as presented by the APro product. (4) Use Level 1 data to chart the satellite overpass trajectories and to acquire topographical information during specific dust events.

The key operational steps are as follows:

(1) To guarantee the superior quality of the CALIPSO LIDAR Level 2 Version 4.2 5 km Aerosol Profile products, three mechanisms of quality control are deployed: the use of the atmospheric volume description (AVD), the CAD score, and the extinction uncertainty parameter, known as extinction QC. These strategies serve to sift through and pinpoint data of utmost dependability. Following this, the information is organized into a three-dimensional grid system, structured at a resolution of $0.5^\circ \times 0.5^\circ \times 500$ m. This organization assists in the detailed examination of the three-dimensional spread of dust aerosol optical data across CA.

Within each grid, the dust extinction coefficient is defined as the ratio of the cumulative sum of the dust extinction coefficient profiles at the same altitude to the number of profiles at that altitude. The formula is as follows:

$$\overline{\sigma_{aer}} = \frac{\sum_{i=1}^{N_q} \sigma_{aer}}{N_Q} \tag{1}$$

In the formula above, σ_{aer} represents the dust aerosol extinction coefficient, while N_Q denotes the number of dust aerosol profiles within the grid.

(2) Frequency of Occurrence of Dust Aerosols

By selecting dust aerosols based on the feature classification information in the VFM categorization products, the frequency of dust occurrence (f) can be calculated. This is achieved by determining the ratio of the number of dust profiles (N_d) within a specific altitude layer of a res $\times$ res grid to the total number of profiles absent of clouds (N_a):

$$f = \frac{N_d}{N_a} \tag{2}$$

(3) Dust Layers

Utilizing the Vertical Feature Mask (VFM) product to identify dust aerosols, we define a dust layer as a continuous altitude layer above each latitude and longitude grid point where only dust aerosols are present [41]. Building on this definition, we have introduced a new concept wherein the continuous altitude minimum threshold is set at 180 m. That is, layers with a continuous height of less than 180 m are not considered as part of the dust layer, retaining only the sections exceeding 180 m in continuous height.

2.3. TROPOMI Data

The Tropospheric Monitoring Instrument (TROPOMI) onboard the Sentinel-5P satellite represents the world's most advanced atmospheric spectrometer to date, boasting the highest spatial resolution and exceptional performance capabilities, with a remarkable potential for aerosol observation [42]. A key differentiator of the TROPOMI sensor (manufactured by Netherlands Organization for Applied Scientific Research, The Hague, The Netherlands) from others lies in its ability to measure across multiple spectral bands (ultraviolet and visible light, near-infrared, and shortwave infrared), allowing for unprecedented precision in imaging a variety of pollutants. The imaging swath of TROPOMI spans up to 2600 km. Initially, its imaging resolution was 7 km $\times$ 3.5 km, which has been enhanced since 6 August 2019 to 5.5 km $\times$ 3.5 km (excluding the UVI and SWIR bands) [43]. This advancement enables daily global coverage and the capability to acquire detailed data on aerosols and clouds. Specifically, for dust observations, the ultraviolet aerosol index (UVAI) measurement technique is employed, providing a quantifiable index indicating the level of aerosols present in the atmosphere. This study utilizes this instrument to aid in the validation of dust pollution processes, as well as the migration and distribution characteristics of dust.

2.4. ERA5-LAND Data

The ERA5-LAND dataset forms part of the ERA5 project, specifically designed to offer high-resolution and high-quality information regarding terrestrial surface states and processes [44]. In this study, the ERA5-LAND/MONTHLY_BY_HOUR dataset was employed, which is updated hourly and made available on a monthly basis. This is aimed at providing an exhaustive temporal resolution to facilitate detailed analysis of meteorological and hydrological conditions within specific periods. The variables selected for this research include surface net solar radiation, u_component_of_wind, v_component_of_wind, surface solar radiation downwards, surface thermal radiation downwards, 2 m temperature, skin temperature, and total precipitation. Furthermore, these variables were processed to yield annual averages, aligned with the years observed by the CALIOP lidar. Additionally, the ERA5-LAND data were processed to a horizontal resolution of 5000 m to maintain consistency with the resolution of CALIOP data.

2.5. HYSPLIT Model

The HYSPLIT-4 is acknowledged as a critical instrument for tracing the spatial routes of air masses from their origin to the point of impact, demonstrating its proficiency in computing and detailing the transport and spread of air pollutants [45]. Owing to its adeptness in managing diverse meteorological inputs and physical dynamics related to pollutant dispersal, the HYSPLIT model is extensively recognized among the atmospheric science community as a leading model for studying atmospheric transport and dispersion. Its functionality encompasses a wide range of scenarios including transport, diffusion, and deposition processes, which make it suitable for simulating various phenomena such as dust, emissions from both stationary and mobile sources, smoke, etc. This versatility enables its widespread use in investigating the movement of atmospheric pollutants [46]. The model employs a static three-dimensional Eulerian grid as the foundational structure for estimating concentrations of air pollutants. By selecting a specific geographical location as the air mass source point, the model facilitates the identification of aerosol sources and

origins for the area under study. For this research, the HYSPLIT model was applied to backtrack and trace air mass trajectories, enhancing the understanding of aerosol sources and predictive pathways during characteristic dust events in the CA territory.

2.6. Random Forest Model

We can simplify this by calling the RF model. Characterized as a nonlinear machine learning approach and an algorithmic mechanism, it is adept at managing and analyzing high-dimensional datasets. Comprising a multitude of decision trees, the RF model leverages the principle of ensemble learning to amalgamate various trees for performing classification and regression tasks, as highlighted in studies by Sun et al. [47]. For regression purposes, random forests select the minimal set of variables for partitioning, with the final output being derived from the average of the outcomes across all decision trees [48,49]. Additionally, the RF model efficiently organizes multiple variables and samples, ranking these variables in terms of their importance and delineating their relative significance [50]. It is particularly effective for handling imbalanced samples by balancing errors, thus preventing overfitting and diminishing the error of generalization. Notably, the RF model bypasses the need for feature selection, is highly adaptable to different datasets and is capable of identifying interactions among various categorical variables throughout the learning and training phases. The model is praised for its swift training capability, facilitating quick assessment of the significance hierarchy among numerous variables, and is thus acknowledged as a superior algorithm in its field. In the context of this research, DOD serves as the primary dependent variable, with the study examining environmental covariates including surface net solar radiation (X1), u-component of wind (X2), v-component of wind (X3), surface solar radiation downwards (X4), surface thermal radiation downwards (X5), 2 m temperature (X6), skin temperature (X7), and total precipitation (X8). Utilizing the framework provided by the random forest (RF) model, this investigation employs these environmental covariates to appraise the DOD values in CA and deduce the significance of each environmental covariate.

3. Results and Analysis

3.1. Three-Dimensional Construction of Optical Parameters

We have conducted a three-dimensional construction of the extinction coefficient, backscatter coefficient, and depolarization ratio of dust aerosols in the CA region. Five horizontal slices were made at elevations corresponding to 0–2 km, 2–4 km, 4–6 km, 6–8 km and 8–10 km, respectively. Through Figure 2, which depicts the seasonal distribution of extinction coefficients, it is apparent that the Taklimakan Desert in Xinjiang, China, maintains high extinction coefficients throughout all seasons. Notably, in spring, the coefficient can reach up to 0.6 km^{-1}, with the area of high values being the widest. In contrast, other regions predominantly exhibit high extinction coefficients concentrated between 0.1 and 0.2 km^{-1}. Furthermore, these high coefficients are primarily found in the lower troposphere (0–2 km), gradually diminishing with altitude, demonstrating a seasonal trend of spring > summer > autumn > winter. Importantly, within the 0–2 km altitude during winter, a high extinction is observed in regions such as central and western Kazakhstan, mainly in a punctiform distribution.

Figure 3 demonstrates that the strong scattering properties of particles are primarily localized in the Taklimakan Desert, with significant changes (notably weakening) as the altitude increases. By integrating the data from Figure 4, it is noted that for dust particles, the degree of irregularity mainly lies between 0.2 and 0.4. Regions above 4 km over Kazakhstan, Uzbekistan, Tajikistan, and Kyrgyzstan exhibit mostly void values, conclusively indicating that dust predominantly accumulates within the 4 km altitude range. The high values during the winter are concentrated within 2 km, largely because of the low subsurface and air temperatures, resulting in a stable atmospheric structure and a reduction in the frequency of strong winds. Furthermore, dust over the Tianshan Mountains mainly spreads across the altitude range of 2–6 km.

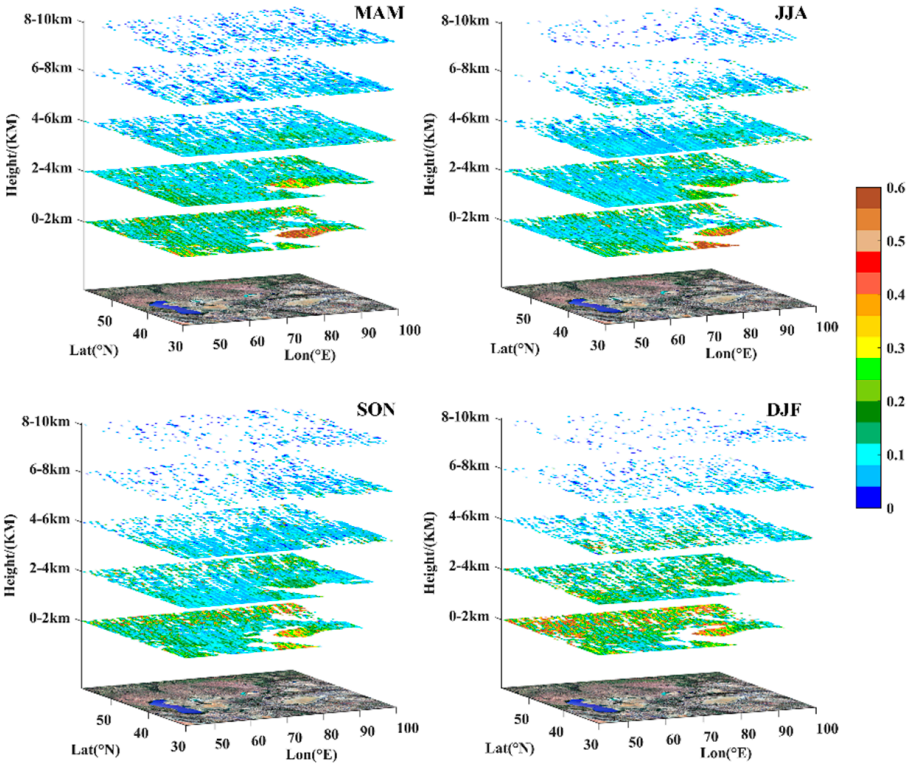

Figure 2. Seasonal distribution of extinction coefficients in CA (km^{-1}).

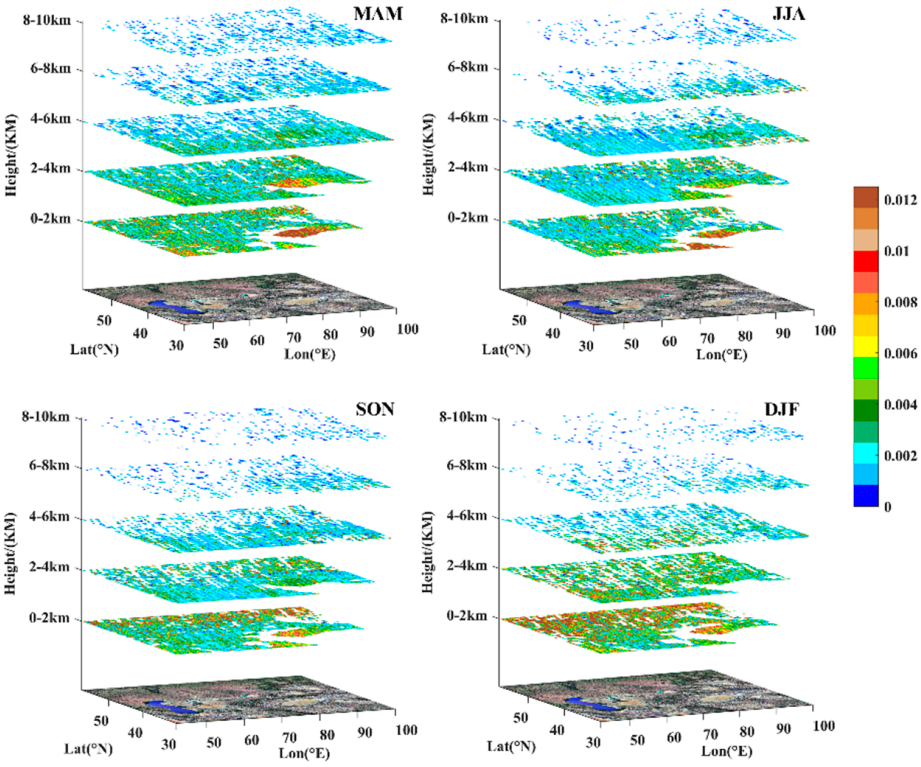

Figure 3. Seasonal distribution of backscatter coefficients in CA ($km^{-1} \cdot sr^{-1}$).

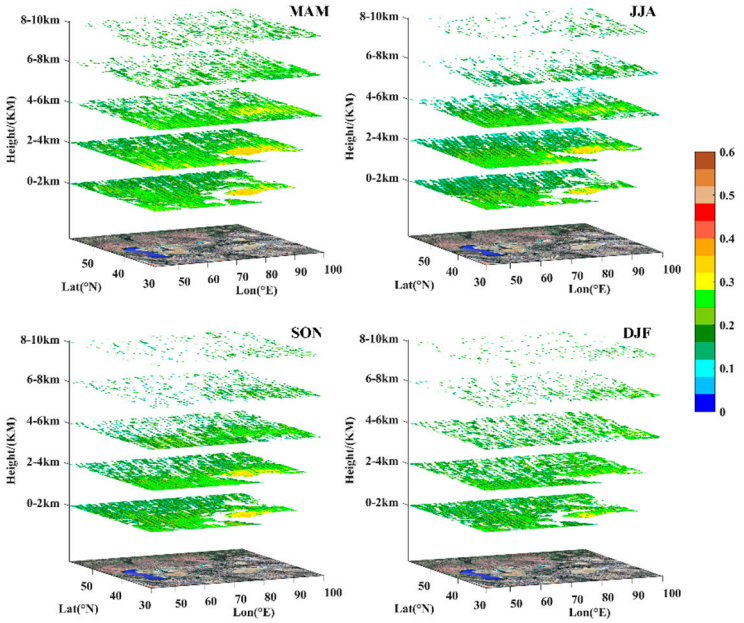

Figure 4. Seasonal distribution of depolarization ratios in CA.

3.2. Frequency of Dust Aerosol Occurrences

Figure 5 illustrates the distribution map of dust occurrence frequencies across the seasons in the CA region. It is clear that the highest frequency of dust events in the Tarim Basin in Xinjiang, China, dominates, averaging over 80% and diminishing gradually toward the outskirts. This pattern is particularly pronounced during the spring and summer months. High occurrence frequencies of dust (80%) in Turkmenistan and Uzbekistan were found to exist in striped patterns, primarily due to the contribution of dust from the Karakum and Kyzylkum deserts. In Kazakhstan, the high frequency of dust occurrences is distributed in a patchy pattern, while in Kyrgyzstan and Tajikistan, high values of dust distribution at altitudes of 2–4 km were observed. The overall region shows a trend of decreasing dust occurrence frequency with increasing altitude and seasonal changes. In summary, the high frequencies of dust occurrences in the CA region are primarily concentrated within latitudes below 42° north, where the sources of dust are richer, thereby promoting the occurrence of high-frequency dust events in areas with these sources.

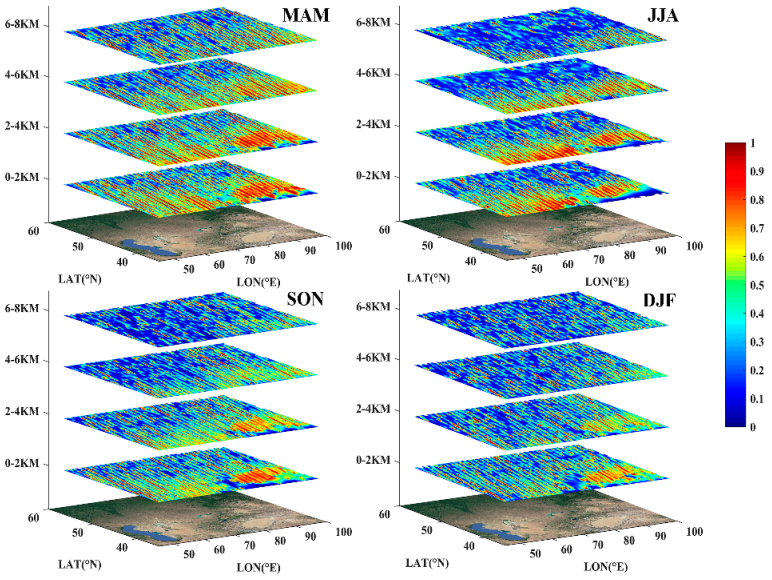

Figure 5. Seasonal distribution of dust occurrence frequency in CA.

3.3. Seasonal Variation in DOD in CA

In this subsection, the selected CALIOP-APRO data are processed to obtain the DOD. The spatial distribution of seasonal and annual average DODs above the CA region is depicted in Figure 6, with the high values (>0.5) within the Taklimakan Desert in Xinjiang, China, being most prevalent in the summer. On the whole, grid points with a DOD greater than 0.25 are more densely distributed in the spring. High values during the summer are also present in Turkmenistan and Uzbekistan, and a small area of high values exists in the western part of Kazakhstan, near the Caspian Sea. Changes in other regions are not significant. This study has quantitatively extracted the seasonal average DOD values for the five countries in CA and Xinjiang, China (see Figure 7). Analyzing the DOD distribution across different regions reveals that Turkmenistan exhibits the highest value among all areas in the summer (0.31), followed by Xinjiang, China, which reaches a high value in spring (0.27). Additionally, Tajikistan, Uzbekistan, and Turkmenistan, all bordering Afghanistan, achieve high DOD values in the summer, while Kazakhstan, Kyrgyzstan, and Xinjiang, China, differ by reaching their highest values in the spring. Viewing the annual average spatial distribution, the DOD in the CA region exhibits a pattern of higher values at the edges and lower values in the middle.

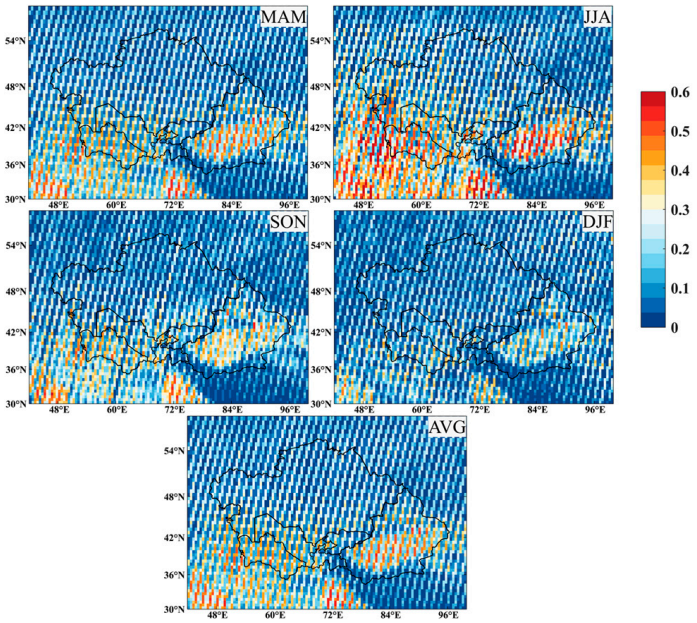

Figure 6. Seasonal and annual average spatial distribution of DOD in CA.

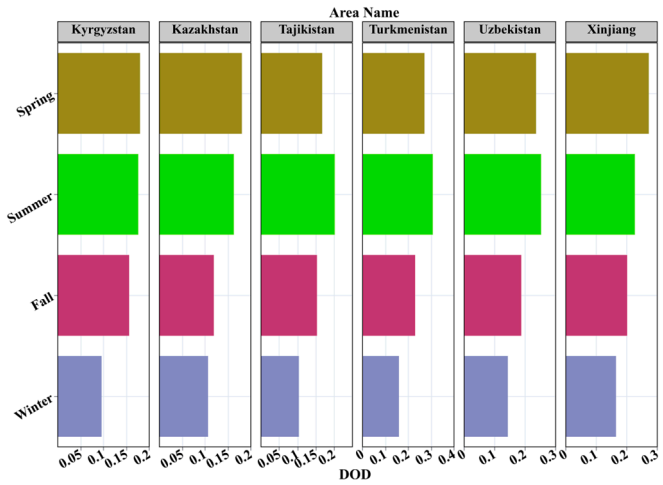

Figure 7. Variation in seasonal mean DOD in five central Asian countries and Xinjiang, China.

This study continues to employ APro data (V4-20 for 2007 to 2021 and V3-41 for 2022) to calculate and plotg the multi-year monthly average spatial distribution maps of DOD over CA (Figure 8). As the figure illustrates, the monthly average high values of DOD in the CA region are significantly noticeable from March to August. Beginning in April, the range of high DOD values expands substantially across most of the CA region, more readily impacting other areas. Simultaneously, distinct high-value zones are observed around the Aral Sea's dried riverbed and its surrounding regions. This phenomenon is associated with an increase in the frequency of strong winds, rising temperatures, and unstable stratification during this period, thereby significantly enhancing regional dust activity. Moreover, the Karakum Desert in Turkmenistan, inside China's Xinjiang Tarim Basin, and the Kyzylkum Desert, primarily located in Uzbekistan, exhibit intense activity during the summer half of the year. In contrast, Kyrgyzstan and Tajikistan, whose geographical locations are largely in mountainous areas, display lower DOD values, mainly below 0.3. By quantitatively extracting the monthly average DOD values of the five CA countries and Xinjiang in China (Figure 9), it is found that Tajikistan, Turkmenistan, and Uzbekistan all reach high DOD values in July during the summer. Kazakhstan and Xinjiang in China, on the other hand, reach their peaks in April during the spring. Additionally, it is crucial to note that Kyrgyzstan reaches its peak value in July, which contradicts its high value in the spring. In other words, this region demonstrates different patterns of high aerosol optical depth (AOD) values for dust in specific seasons and months. The details of this exploration are discussed in the discussion section.

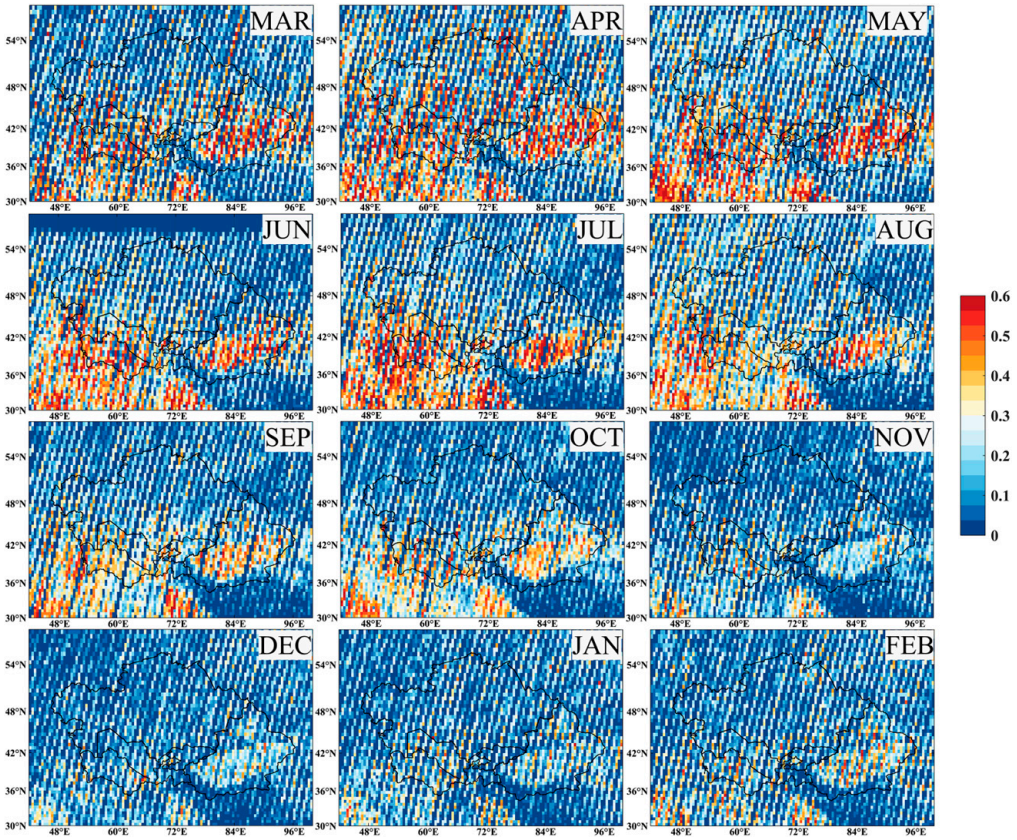

Figure 8. Monthly average spatial distribution variation in DOD in CA.

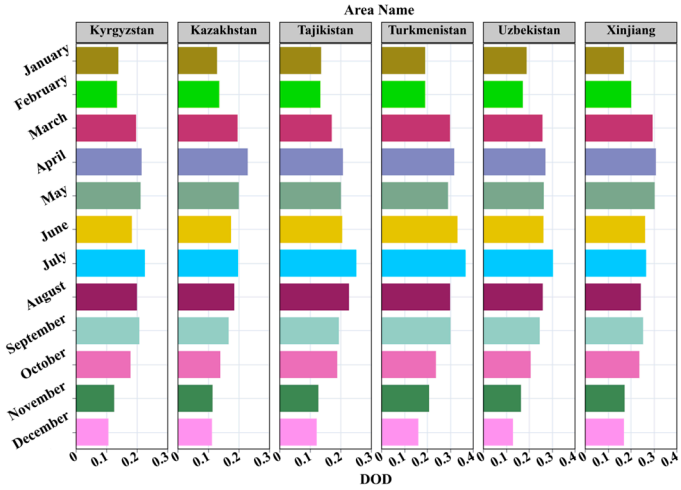

Figure 9. Variation in monthly mean DOD in five central Asian countries and Xinjiang, China.

3.4. Characteristics of the Dust Layer

CALIOP VFM data were processed to analyze the characteristics of the dust layer's distribution over CA. For the methodology, refer to Section 2.2 (3). Figure 10 depicts the seasonal and annual average of the top altitude of the dust layer, the base altitude of the dust layer, and the thickness of the dust layer across CA for the years 2007–2022. In the spring, the top altitude of the dust layer in the southern region of Xinjiang, China, is relatively high (4–6 km), whereas in the five CA countries, it is primarily concentrated at an altitude of 2–4 km, gradually decreasing with the season change. The base altitude of the dust layer is mainly concentrated within 2 km throughout the seasons. Regarding the thickness of the dust layer, in the spring and summer, in the major areas of the Taklimakan Desert, the thickness is concentrated above 3 km, while in Turkmenistan and Uzbekistan, it is mainly above 2 km, with the rest of the regions having dust layers with a 1 km thickness across all seasons. Looking at the annual average spatial distribution, the top altitude of the dust layer in the southern region of Xinjiang, China, is concentrated at a height of 4 km, with other areas being less than 3 km. As for the base altitude of the dust layer, it is below 2 km across CA. In terms of the thickness of the dust layer, most of the southern region of Xinjiang, China, the thickness is concentrated at 2 km, followed by Turkmenistan and Uzbekistan, with a dust thickness concentrated at 1–2 km, while that in other regions is less than 1 km. From the perspective of dust transport, the large deserts within Turkmenistan and Uzbekistan have ample sand sources. Under the action of thermodynamics and dynamics, they transport dust to surrounding areas. Hence, the dust layer in the southwestern part of Kazakhstan, bordering Uzbekistan, is relatively thicker compared to other areas.

Moreover, we have quantitatively calculated the annual thickness of the dust layer for the five CA countries and China's Xinjiang from 2007 to 2022 (see Figure 11a). The figure reveals that the thickness of the dust layer in Turkmenistan has been higher than that in other areas over the past 16 years. The order of the thickness of the dust layer from high to low in other regions is as follows: Uzbekistan > Kazakhstan > Tajikistan > Kyrgyzstan > Xinjiang, China. Through Figure 11b–d, all five CA countries and China's Xinjiang have passed the significance test with a 95% confidence level over the past 16 years, showing an upward trend. Moreover, the thickness of the dust layer from high to low is as follows: Turkmenistan (1.07 km), Uzbekistan (0.91 km), Kazakhstan (0.70 km), Tajikistan (0.53 km), Kyrgyzstan (0.47 km), and Xinjiang, China (0.30 km). In terms of the thickness of the dust layer over the research period in the study area, a dust layer exists over CA with an average thickness of approximately 0.62 km. This also indirectly reflects the severity of the atmospheric pollution problem posed by dust aerosols.

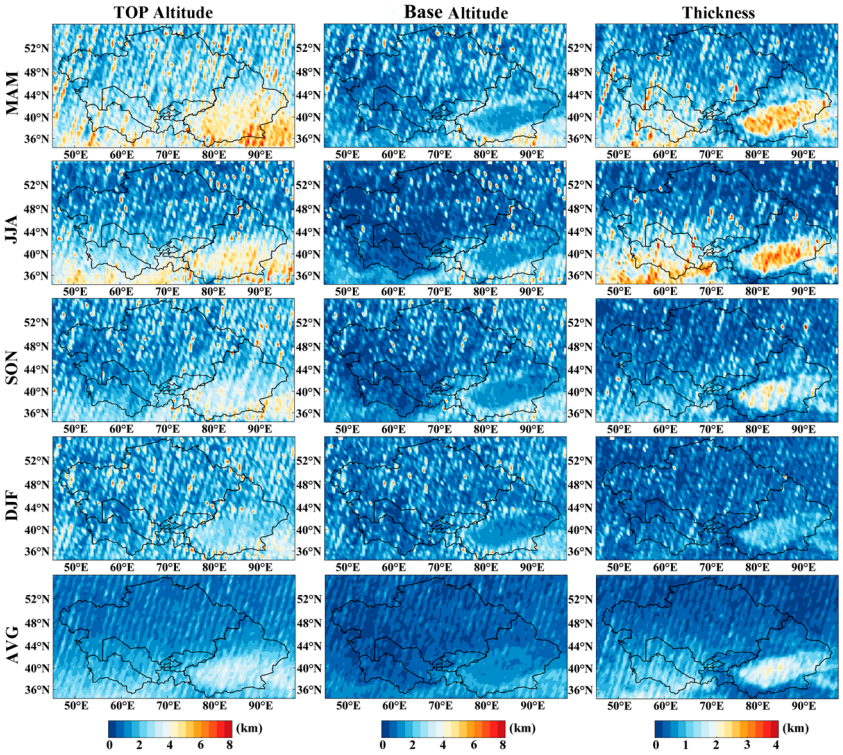

Figure 10. Seasonal and annual average spatial distribution of dust layers in CA.

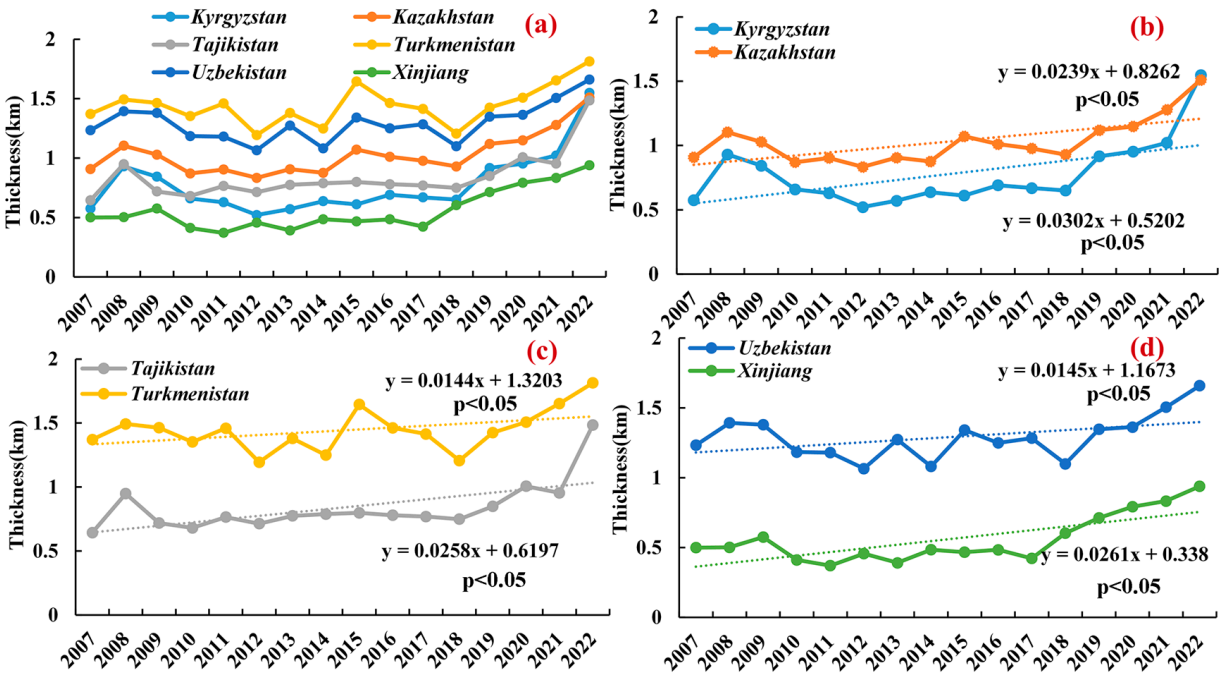

Figure 11. (**a**) shows the multi-year trends in dust layer thickness for the five Central Asian countries and Xinjiang, China. (**b**–**d**) show the trends in dust layer thickness for the two regions, respectively.

3.5. Case Analysis of Dust Transport

This section focuses on monitoring dust transport processes using CALIOP-APro and VFM data through remote sensing. The extinction coefficient serves as an indicator of the atmospheric particulate concentration, with higher values indicating greater concentrations of suspended particulate matter. The VFM product, on the other hand, is employed to differentiate between the types of aerosols present in the atmosphere.

Through the analysis of Figure 12b, a dust weather event was detected in the region of Kyrgyzstan in CA on 18 April. The extinction coefficient values measured in this area ranged from 0.1 to 0.2 km^{-1}. Coupled with VFM classification results, it was determined that the aerosols above this mountainous area were predominantly dust aerosols. Further observations of the mountain area on the morning of 19 April confirmed the continuous presence of dust aerosols. Satellite observations showed that within a 1km height range above the Tien Shan, extinction values could reach up to 0.6 km^{-1}, decreasing with an increasing altitude. By 20 April, the observation point was moved eastward to track the dust transport path, as shown in the satellite trajectory in Figure 12g, where the extinction coefficient values were detected above the east side of the Tianshan mountain range. Combined with the analysis of Figure 12i, it was found that there was a mixture of dust and pollution-related dust aerosols in the region, with a vertical distribution up to 6 km in height. Moreover, observation data indicated the presence of a thick dust layer within the Tarim Basin in Xinjiang, China, with a vertical distribution reaching up to the top of the troposphere (about 8 km height), providing sufficient conditions for long-distance dust transport. The classification results from Figure 12c,f,i reveal a 4 to 6 km thick dust layer over the Tarim Basin.

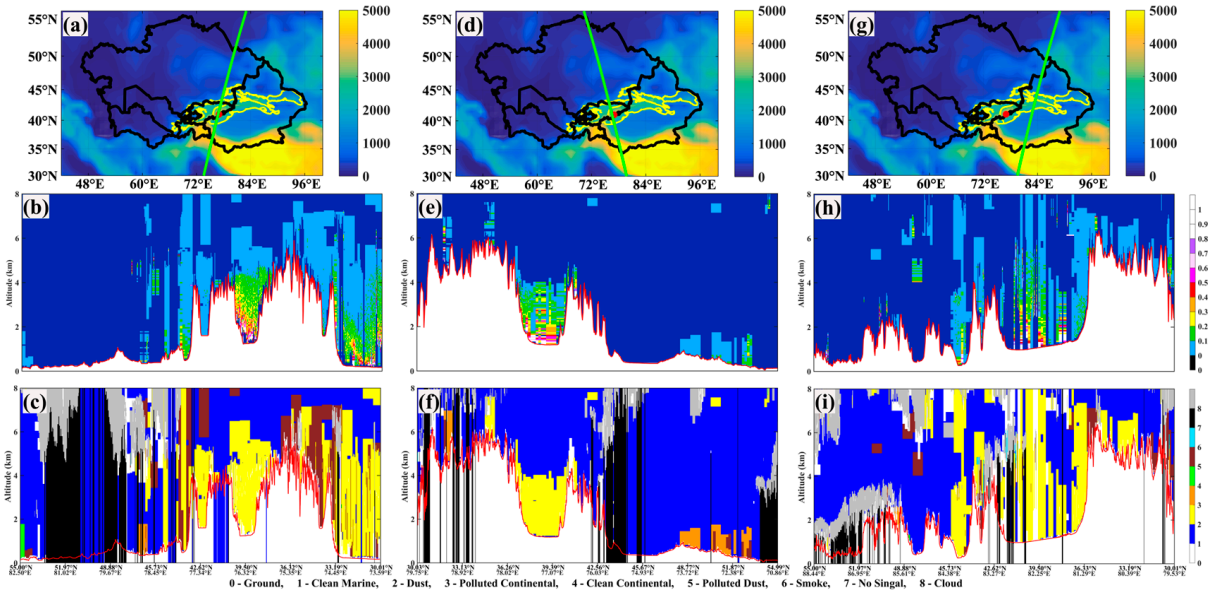

Figure 12. Panels (**a**), (**d**), and (**g**) display the CALIPSO satellite trajectories over the CA region on 18, 19 and 20 April 2022, respectively. Panels (**b**,**e**,**h**) show the extinction coefficients observed by CALIPSO (corresponding to the satellite's overpass times), while panels (**c**,**f**,**i**) present the altitude–satellite orbit profiles of aerosol type classification results (corresponding to the satellite overpass times). Note: The red solid line represents the ground level, white represents the terrain, and the red dots indicate locations in the mountainous regions of Kyrgyzstan.

The UVAI index is an indicator used to measure the presence of absorbent aerosols in the atmosphere. It is crucial for detecting dust events. The distribution of UVAI values observed by the TROPOMI sensor indicates the presence of absorbent aerosols starting from 18 April in southeastern Kazakhstan, Kyrgyzstan, Tajikistan, and the southern part of Xinjiang, China (see Figure 13a). The UVAI values for the CALIPSO satellite's transit trajectories on 19 and 20 April, as depicted in Figure 13b,c, correspond with the observed dust activities. This is particularly evident in areas where the UVAI values exceeded 1, indicating a strong distribution of absorbing aerosols.

In summary, combining observations from CALIPSO and TROPOMI indicates a clear process of dust transport from CA across the Tianshan mountains to the east. Although the concentration of dust decreases, its transport process can still be effectively tracked.

To further investigate the sources of dust aerosols over CA and to predict their potential impact areas, this study utilizes the HYSPLIT trajectory model to perform 72 h forward and backward trajectory simulations. The simulations are centered in the mountainous regions of Kyrgyzstan in CA (77°E, 42°N), with the backward simulation covering 15–18 April 2022, and the forward simulation from 18 to 21 April 2022. The results of the simulations are presented in Figure 14a,b.

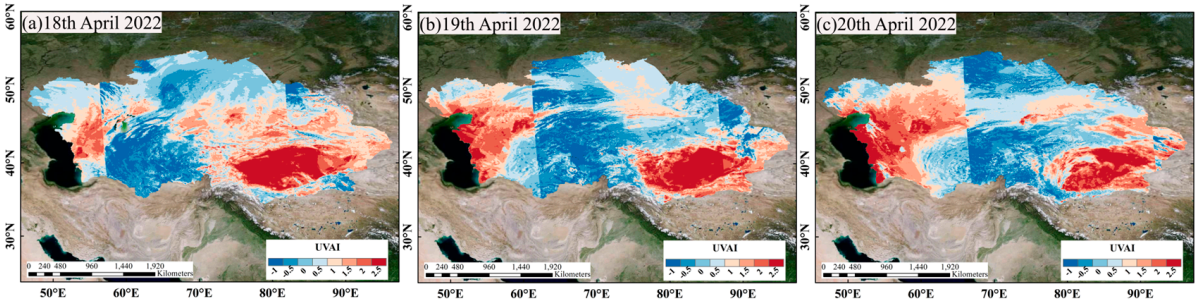

Figure 13. UVAI distribution in the study area observed by TROPOMI from 18 to 20 April 2022.

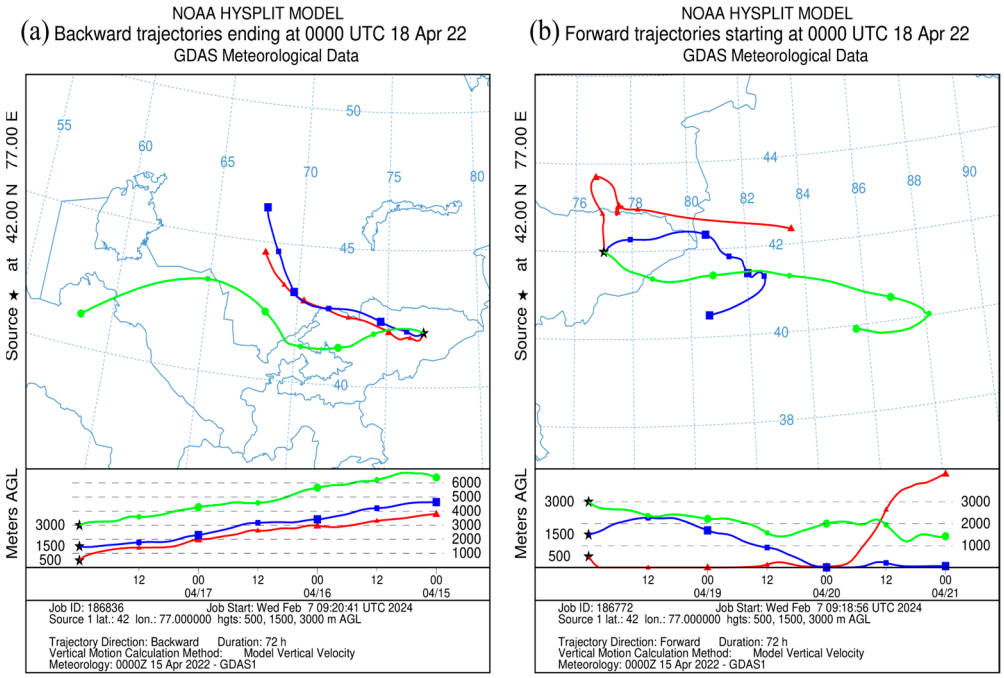

Figure 14. Trajectories of the study site simulated by the HYSPLIT trajectory model for 72 h backward (**a**) and 72 h forward (**b**). Note: The red, blue, and green lines, respectively, represent the forward and backward trajectory lines at elevations of 500 m, 1500 m, and 3000 m above the location point.

The backward trajectory (Figure 14a) reveals that pollutants at heights of 500 m and 1500 m originate from the mid-southern region of Kazakhstan, primarily characterized by desert, semi-desert, and arid areas. The airflow moves from the northwest to the southeast direction, with the particle height gradually decreasing, eventually accumulating at the 500 m and 1500 m positions in the Kyrgyzstan mountains. Pollutants at the height of 3000 m are mainly derived from the Karakum Desert in Turkmenistan. On 15 April, dust particles from the surface of the Karakum Desert were lifted by strong winds, with the airflow moving from the southwest to the northeast direction. During this period, dust from the Kyzylkum Desert within Uzbekistan and the southernmost part of Kazakhstan continued to supplement this dust flow. The northwestern airflow carried the pollutants towards Kyrgyzstan, eventually accumulating at a mountainous position of 3000 m. It is clear that the sources of this dust event are mainly desert and semi-desert areas of Kazakhstan, as

well as distant contributions from the Karakum and Kyzylkum Deserts, largely because these regions have extensive desert coverage, are in arid zones, receive little precipitation, and have sufficient conditions for dust uplift.

Figure 14b depicts the forward trajectory lines for the simulated location. Beginning on 18 April, the air mass at a height of 500 m starts moving in a northeast direction, entering the southern region of Kazakhstan before adopting a circular path southward. At the southern border of Kazakhstan, the air mass transitions to a west-to-east movement, and by 20 April, this air mass is rapidly elevated to heights exceeding 3000 m, eventually reaching the northeastern edge of the Aksu region. At an altitude of 1500 m, the air mass moves from west to east into the Xinjiang region of China, gradually descending from the afternoon of 18 April, coming to a stop near the city of Alar. Meanwhile, at a height of 3000 m, under the continuous influence of westerly winds, the air mass maintains a relatively stable posture for long-distance movement. After reaching the central area of the Bayingolin Mongol Autonomous Prefecture, it moves in a circular pattern back towards the west, ultimately affecting the western regions of the prefecture.

3.6. Importance Ranking and Correlation Analysis of Natural Factors

In this study, the random forest (RF) model and correlation analysis methods were employed to elucidate the relationship between DOD and environmental covariates in the CA region. The investigation positions DOD as the dependent variable, incorporating eight meteorological covariates as independent variables into the RF model for analysis.

According to the outcomes of the random forest model, as illustrated in Figure 15a, it was found that the meteorological covariate X7 (skin temperature) has the most significant impact on the DOD, with an importance score of 24.74%, followed by X6 (2m temperature), which exerts an influence of 23.96%. This indicates that X7 and X6 are critical factors affecting DOD variability in CA. Further, the correlation analysis results, depicted in Figure 15b, revealed a significant negative correlation between DOD and X7, with a correlation coefficient of −0.35. Simultaneously, DOD and X6 also exhibit a negative correlation, evidenced by a correlation coefficient of −0.31. These findings bolster the insights from the RF model analysis, signifying that X7 and X6 are the primary drivers of DOD variability in the CA region.

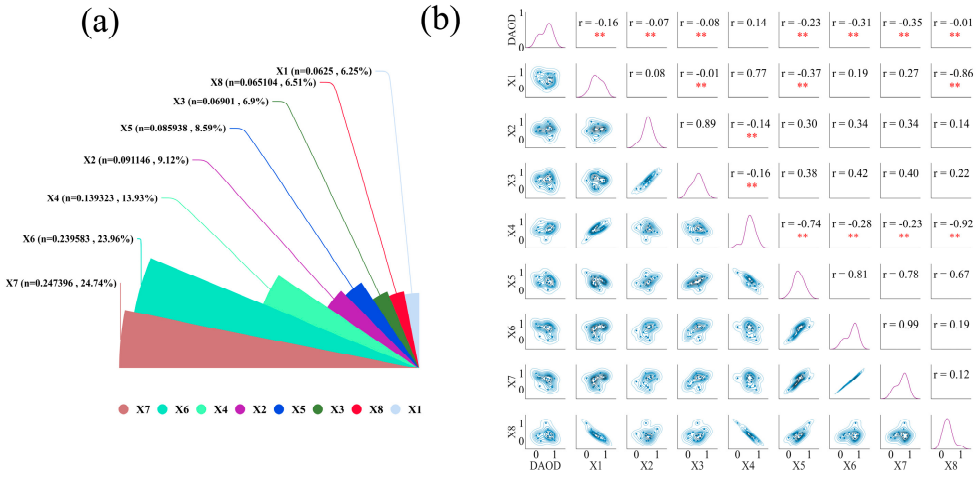

Figure 15. (**a**) RF simulation results and (**b**) correlation results. ** represents $p < 0.01$.

Synthesizing the results from the random forest model and correlation analysis, it can be concluded that X7 and X6 play pivotal roles in influencing the distribution and concentration of dust aerosols in CA, with other variables also contributing to regional dust activities to varying degrees.

4. Discussion

This research primarily utilized CALIPSO satellite data for a three-dimensional analysis of dust aerosols in the CA region. Given the scant precipitation received in CA, vast expanses are covered by desert and semi-desert climates [51], including renowned deserts like Karakum and Kyzylkum [52]. In such areas, cloud coverage is minimal, resulting in clearer skies, which facilitate easier detection of aerosol signals via lidar. Importantly, CALIPSO can effectively distinguish dust layers vertically and even detect instances of long-range dust transport. A key aspect is that CALIPSO provides instantaneous data for specific orbital crossings, and the limited variability in weather conditions in arid regions implies that these data remain representative over extended periods.

Nonetheless, ground validation is also critical to ensure the accuracy and reliability of CALIPSO. We hope to establish more ground-based lidar stations across CA in the future for aerosol monitoring, thus enhancing our analysis of dust distribution and transportation processes in the region. Integrating ground-based lidar data with satellite observations will allow for more comprehensive and detailed observations of the atmospheric aerosol distribution and its dynamic changes, thereby increasing the precision of model forecasts. Importantly, we aim to strengthen scientific cooperation with more countries in CA. Agreements have already been made with some universities and scientific institutions in CA to share monitoring data and outcomes collaboratively, addressing and mitigating regional and global climate change together.

This study identified an intriguing phenomenon where certain CA nations exhibit distinct high-value AOD patterns during specific seasons and months. Especially noteworthy is Kyrgyzstan, where seasonal highs appear in spring, yet the highest monthly mean AOD is found in July. This discrepancy could stem from several possible causes: (1) CA's windy season predominantly occurs in April, aiding in dust uplift and transport. Kyrgyzstan, with its unique terrain and climate, might experience significant dust contributions from local or nearby deserts, such as the Kyzylkum Desert, in spring. (2) Although spring is a dust-prone season, the high monthly mean AOD values in July could result from a combination of factors, including persistent drought conditions or dust from distant sources impacting Kyrgyzstan through atmospheric transport in certain years. (3) Data statistics and computational methods. Statistical treatment of monthly versus seasonal averages may reveal different trends. For instance, intense dust storms in July might significantly impact monthly averages, despite spring being overall more susceptible to dust. Additionally, Kyrgyzstan's predominantly mountainous terrain could affect the pathways and settling patterns of dust to some extent, particularly in summer when dust transported over long distances might accumulate in specific areas within Kyrgyzstan. Future studies should closely monitor dust events in this region.

The research also demonstrated that the three environmental variables most significantly correlated with the DOD are skin temperature, temperature at 2 m, and surface thermal radiation downwards, all of which show clear negative correlations. This might be because temperatures at 2 m and skin temperature typically reflect atmospheric instability near the ground, facilitating vertical air currents leading to aerosol upward transport, reducing near-surface aerosol concentrations. Under cooler conditions, especially in winter, low temperatures could slow down the drying processes at dust sources or dry surfaces, thereby reducing the amount of dust entering the atmosphere. Furthermore, a decrease in surface thermal radiation downwards could occur because aerosols increase the atmosphere's opacity, leading to the partial absorption and scattering of radiation. However, these explanations are not conclusively accurate, and we hope to conduct longer-term observations in the future, also taking into account more variables such as atmospheric composition and land use.

In conclusion, through CALIPSO satellite data, this study conducted a detailed analysis of the three-dimensional distribution and dynamic changes in dust aerosols in CA. Moreover, using ERA5-LAND, it unveiled the complex interactions between dust and several environmental variables such as skin temperature, 2 m temperature, and surface

thermal radiation downwards. With the gradual establishment of ground observation networks and deepened international cooperation, we hope to provide more accurate predictive models in the future, offering a solid scientific foundation for understanding the impact of aerosols on climate change in CA and globally. Further evaluating the interactions between key environmental variables and dust aerosols will not only aid in predicting dust storm occurrences and their pathways but also provide critical scientific support for mitigating the impact of dust storms on regional and global environments and societies.

5. Conclusions

This study utilized CALIOP lidar data to construct a three-dimensional distribution of dust aerosols in CA from 2007 to 2022. The results indicate that the distribution of dust aerosols in CA exhibits significant seasonal variations throughout the year. Specifically, the Taklimakan Desert in Xinjiang, China, displayed a high extinction coefficient (up to 0.6 km^{-1}) in spring, reflecting the intensity of dust activity during this season. Moreover, the frequency of dust occurrences in Xinjiang's Tarim Basin exceeded 80% on average during the spring and summer months, with high dust frequencies also observed in the Karakum and Kyzylkum Deserts. These findings further reveal the impact of geographical location on the intensity of dust activity in CA.

Turkmenistan reached the highest seasonal mean DOD (0.31) of all regions in CA during summer, followed by Xinjiang (0.27), demonstrating the significant seasonal differences across the area. Meanwhile, monthly mean DOD data highlight March to August as the primary months for high DOD values in CA, with a 0.62 km thick dust layer present over the region. Additionally, spring and summer are the seasons with the thickest dust layers, especially over desert zones like the Taklimakan Desert and Karakum Desert. Trajectory models have confirmed that dust transport in CA can cross the Tianshan mountains, affecting eastern regions. Furthermore, skin temperature is identified as the most significant factor influencing the DOD in CA and is negatively correlated with it.

This work uncovers the long-term spatial and temporal distribution features of dust aerosols in the CA region, showcasing the potential of CALIOP for analyzing the three-dimensional attributes of dust. By integrating multiple sources of data and employing machine learning techniques, it identifies natural elements that play significant roles in the dynamic distribution of dust. Our future research will be dedicated to utilizing more advanced climate models and satellite remote sensing technologies to refine the source–sink processes of dust aerosols. We aim to delve deeper into their impact on public health and climate change and to develop more accurate dust storm warning systems, thereby providing a more tangible and effective scientific foundation for the formulation of regional environmental policies.

Author Contributions: J.L.: Software, Writing—original draft and Writing—review and editing; Y.W.: Investigation, Project administration and Funding acquisition; Q.H.: Conceptualization, Methodology and Supervision; X.M.: Data curation and Software; X.Z.: Investigation; Y.L.: Software. All authors have read and agreed to the published version of the manuscript.

Funding: This research was funded by the Regional Collaborative Innovation Program of Xinjiang Province (Grant No. 2022E01014); the Tianchi Talent Introduction Programme (Young Doctor); the National Natural Science Foundation of China (Grant No. 42030612); and the Third Xinjiang Scientific Expedition and Research program (Grant No. 2021xjkk030501).

Data Availability Statement: The CALIPSO-CALIOP data are available at https://subset.larc.nasa.gov/calipso/login.php (accessed on 2 October 2023) and the ERA5-LAND data are available at https://cds.climate.copernicus.eu/ (accessed on 2 March 2024).

Acknowledgments: We would like to thank the Urumqi Desert Meteorological Institute of China Meteorological Administration for their support.

Conflicts of Interest: The authors declare no conflicts of interest.

References

1. Li, H.; Yang, Y.; Wang, H.; Wang, P.; Yue, X.; Liao, H. Projected aerosol changes driven by emissions and climate change using a machine learning method. *Environ. Sci. Technol.* **2022**, *56*, 3884–3893. [CrossRef] [PubMed]
2. Cheng, Y.; Dai, T.; Li, J.; Shi, G. Measurement Report: Determination of aerosol vertical features on different timescales over East Asia based on CATS aerosol products. *Atmos. Chem. Phys.* **2020**, *20*, 15307–15322. [CrossRef]
3. Li, B.; Gasser, T.; Ciais, P.; Piao, S.; Tao, S.; Balkanski, Y.; Hauglustaine, D.; Boisier, J.-P.; Chen, Z.; Huang, M. The contribution of China's emissions to global climate forcing. *Nature* **2016**, *531*, 357–361. [CrossRef] [PubMed]
4. Huang, J.; Wang, T.; Wang, W.; Li, Z.; Yan, H. Climate effects of dust aerosols over East Asian arid and semiarid regions. *J. Geophys. Res. Atmos.* **2014**, *119*, 11–398. [CrossRef]
5. Bi, J.; Huang, J.; Hu, Z.; Holben, B.N.; Guo, Z. Investigating the aerosol optical and radiative characteristics of heavy haze episodes in Beijing during January of 2013. *J. Geophys. Res. Atmos.* **2014**, *119*, 9884–9900. [CrossRef]
6. Liu, Y.; Shi, G.; Xie, Y. Impact of dust aerosol on glacial-interglacial climate. *Adv. Atmos. Sci.* **2013**, *30*, 1725–1731. [CrossRef]
7. Zhang, H.; Ma, J.; Zheng, Y. Modeling study of the global distribution of radiative forcing by dust aerosol. *Acta Meteorol. Sin.* **2010**, *24*, 558–570.
8. Rosenfeld, D.; Lohmann, U.; Raga, G.B.; O'Dowd, C.D.; Kulmala, M.; Fuzzi, S.; Reissell, A.; Andreae, M.O. Flood or drought: How do aerosols affect precipitation? *Science* **2008**, *321*, 1309–1313. [CrossRef] [PubMed]
9. Li, Z.; Niu, F.; Fan, J.; Liu, Y.; Rosenfeld, D.; Ding, Y. Long-term impacts of aerosols on the vertical development of clouds and precipitation. *Nat. Geosci.* **2011**, *4*, 888–894. [CrossRef]
10. Tao, W.K.; Chen, J.P.; Li, Z.; Wang, C.; Zhang, C. Impact of aerosols on convective clouds and precipitation. *Rev. Geophys.* **2012**, *50*, 2. [CrossRef]
11. Ding, A.J.; Fu, C.B.; Yang, X.Q.; Sun, J.N.; Petäjä, T.; Kerminen, V.M.; Wang, T.; Xie, Y.; Herrmann, E.; Zheng, L.F. Intense atmospheric pollution modifies weather: A case of mixed biomass burning with fossil fuel combustion pollution in eastern China. *Atmos. Chem. Phys.* **2013**, *13*, 10545–10554. [CrossRef]
12. Ackerman, A.S.; Toon, O.B.; Stevens, D.E.; Heymsfield, A.J.; Ramanathan, V.; Welton, E.J. Reduction of tropical cloudiness by soot. *Science* **2000**, *288*, 1042–1047. [CrossRef]
13. Huang, J.; Lin, B.; Minnis, P.; Wang, T.; Wang, X.; Hu, Y.; Yi, Y.; Ayers, J.K. Satellite-based assessment of possible dust aerosols semi-direct effect on cloud water path over East Asia. *Geophys. Res. Lett.* **2006**, *33*, 19. [CrossRef]
14. Haywood, J.M.; Abel, S.J.; Barrett, P.A.; Bellouin, N.; Blyth, A.; Bower, K.N.; Brooks, M.; Carslaw, K.; Che, H.; Coe, H. The CLoud–Aerosol–Radiation interaction and forcing: Year 2017 (CLARIFY-2017) measurement campaign. *Atmos. Chem. Phys.* **2021**, *21*, 1049–1084. [CrossRef]
15. Meng, L.; Yang, X.; Zhao, T.; He, Q.; Mamtimin, A.; Wang, M.; Huo, W.; Yang, F.; Zhou, C.; Pan, H. Simulated regional transport structures and budgets of dust aerosols during a typical springtime dust storm in the Tarim Basin, Northwest China. *Atmos. Res.* **2020**, *238*, 104892. [CrossRef]
16. Ginoux, P.; Prospero, J.M.; Gill, T.E.; Hsu, N.C.; Zhao, M. Global-scale attribution of anthropogenic and natural dust sources and their emission rates based on MODIS Deep Blue aerosol products. *Rev. Geophys.* **2012**, *50*, 3. [CrossRef]
17. Schuster, G.L.; Dubovik, O.; Arola, A. Remote sensing of soot carbon–Part 1: Distinguishing different absorbing aerosol species. *Atmos. Chem. Phys.* **2016**, *16*, 1565–1585. [CrossRef]
18. Zhu, Q.; Liu, Y.; Jia, R.; Hua, S.; Shao, T.; Wang, B. A numerical simulation study on the impact of smoke aerosols from Russian forest fires on the air pollution over Asia. *Atmos. Environ.* **2018**, *182*, 263–274. [CrossRef]
19. Chen, X.; Ding, J.; Liu, J.; Wang, J.; Ge, X.; Wang, R.; Zuo, H. Validation and comparison of high-resolution MAIAC aerosol products over Central Asia. *Atmos. Environ.* **2021**, *251*, 118273. [CrossRef]
20. Indoitu, R.; Kozhoridze, G.; Batyrbaeva, M.; Vitkovskaya, I.; Orlovsky, N.; Blumberg, D.; Orlovsky, L. Dust emission and environmental changes in the dried bottom of the Aral Sea. *Aeolian Res.* **2015**, *17*, 101–115. [CrossRef]
21. Zhang, X.-X.; Claiborn, C.; Lei, J.-Q.; Vaughan, J.; Wu, S.-X.; Li, S.-Y.; Liu, L.-Y.; Wang, Z.-F.; Wang, Y.-D.; Huang, S.-Y. Aeolian dust in Central Asia: Spatial distribution and temporal variability. *Atmos. Environ.* **2020**, *238*, 117734. [CrossRef]
22. Miller-Schulze, J.P.; Shafer, M.M.; Schauer, J.J.; Solomon, P.A.; Lantz, J.; Artamonova, M.; Chen, B.; Imashev, S.; Sverdlik, L.; Carmichael, G.R. Characteristics of fine particle carbonaceous aerosol at two remote sites in Central Asia. *Atmos. Environ.* **2011**, *45*, 6955–6964. [CrossRef]
23. Chen, B.B.; Sverdlik, L.G.; Imashev, S.A.; Solomon, P.A.; Lantz, J.; Schauer, J.J.; Shafer, M.M.; Artamonova, M.S.; Carmichael, G.R. Lidar measurements of the vertical distribution of aerosol optical and physical properties over Central Asia. *Nat. Geosci.* **2013**, *2013*, 261546. [CrossRef]
24. Hofer, J.; Ansmann, A.; Althausen, D.; Engelmann, R.; Baars, H.; Fomba, K.W.; Wandinger, U.; Abdullaev, S.F.; Makhmudov, A.N. Optical properties of Central Asian aerosol relevant for spaceborne lidar applications and aerosol typing at 355 and 532 nm. *Atmos. Chem. Phys.* **2020**, *20*, 9265–9280. [CrossRef]
25. Xi, X.; Sokolik, I.N. Dust interannual variability and trend in Central Asia from 2000 to 2014 and their climatic linkages. *J. Geophys. Res. Atmos.* **2015**, *120*, 12–175. [CrossRef]
26. Groll, M.; Opp, C.; Aslanov, I. Spatial and temporal distribution of the dust deposition in Central Asia–results from a long term monitoring program. *Aeolian Res.* **2013**, *9*, 49–62. [CrossRef]

27. Bai, J.; Chen, X.; Li, J.; Yang, L.; Fang, H. Changes in the area of inland lakes in arid regions of central Asia during the past 30 years. *Environ. Monit. Assess.* **2011**, *178*, 247–256. [CrossRef] [PubMed]
28. Issanova, G.; Abuduwaili, J.; Galayeva, O.; Semenov, O.; Bazarbayeva, T. Aeolian transportation of sand and dust in the Aral Sea region. *Int. J. Environ. Sci. Technol.* **2015**, *12*, 3213–3224. [CrossRef]
29. Li, J.; He, Q.; Ge, X. Spatiotemporal distribution of aerosols over the Tibet Plateau and Tarim Basin (1980–2020). *J. Clean. Prod.* **2022**, *374*, 133958. [CrossRef]
30. Wang, T.; Chen, Y.; Gan, Z.; Han, Y.; Li, J.; Huang, J. Assessment of dominating aerosol properties and their long-term trend in the Pan-Third Pole region: A study with 10-year multi-sensor measurements. *Atmos. Environ.* **2020**, *239*, 117738. [CrossRef]
31. Ge, J.M.; Huang, J.P.; Xu, C.P.; Qi, Y.L.; Liu, H.Y. Characteristics of Taklimakan dust emission and distribution: A satellite and reanalysis field perspective. *J. Geophys. Res. Atmos.* **2014**, *119*, 11–772. [CrossRef]
32. Liu, Z.; Liu, D.; Huang, J.; Vaughan, M.; Uno, I.; Sugimoto, N.; Kittaka, C.; Trepte, C.; Wang, Z.; Hostetler, C. Airborne dust distributions over the Tibetan Plateau and surrounding areas derived from the first year of CALIPSO lidar observations. *Atmos. Chem. Phys.* **2008**, *8*, 5045–5060. [CrossRef]
33. Xu, C.; Ma, Y.M.; You, C.; Zhu, Z.K. The regional distribution characteristics of aerosol optical depth over the Tibetan Plateau. *Atmos. Chem. Phys.* **2015**, *15*, 12065–12078. [CrossRef]
34. Pan, H.; Huo, W.; Wang, M.; Zhang, J.; Meng, L.; Kumar, K.R.; Devi, N.L. Insight into the climatology of different sand-dust aerosol types over the Taklimakan Desert based on the observations from radiosonde and A-train satellites. *Atmos. Environ.* **2020**, *238*, 117705. [CrossRef]
35. Zeng, X.; Li, S.; Xing, J.; Yang, J.; Wang, Q.; Song, G.; Teng, M.; Zhou, D.; Lu, J. CALIPSO-observed Southeast Asia biomass-burning influences on aerosol vertical structure in Guangdong-Hong Kong-Macao Greater Bay Area. *Atmos. Res.* **2023**, *289*, 106755. [CrossRef]
36. Han, Y.; Wang, T.; Tan, R.; Tang, J.; Wang, C.; He, S.; Dong, Y.; Huang, Z.; Bi, J. CALIOP-based quantification of Central Asian dust transport. *Remote Sens.* **2022**, *14*, 1416. [CrossRef]
37. Ma, W.; Ding, J.; Wang, J.; Zhang, J. Effects of aerosol on terrestrial gross primary productivity in Central Asia. *Atmos. Environ.* **2022**, *288*, 119294. [CrossRef]
38. Dou, X.; Ma, X.; Zhao, C.; Li, J.; Yan, Y.; Zhu, J. Risk assessment of soil erosion in Central Asia under global warming. *Catena* **2022**, *212*, 106056. [CrossRef]
39. Hu, Y.; Kang, S.; Yang, J.; Ji, Z.; Rupakheti, D.; Yin, X.; Du, H. Impact of atmospheric circulation patterns on properties and regional transport pathways of aerosols over Central-West Asia: Emphasizing the Tibetan Plateau. *Atmos. Res.* **2022**, *266*, 105975. [CrossRef]
40. Ma, X.; Ding, Y.; Shi, H.; Yan, W.; Dou, X.; Ochege, F.U.; Luo, G.; Zhao, C. Spatiotemporal variations in aerosol optical depth and associated risks for populations in the arid region of Central Asia. *Sci. Total Environ.* **2022**, *816*, 151558. [CrossRef]
41. Xu, X.; Wu, H.; Yang, X.; Xie, L. Distribution and transport characteristics of dust aerosol over Tibetan Plateau and Taklimakan Desert in China using MERRA-2 and CALIPSO data. *Atmos. Environ.* **2020**, *237*, 117670. [CrossRef]
42. Michailidis, K.; Koukouli, M.-E.; Balis, D.; Veefkind, J.P.; De Graaf, M.; Mona, L.; Papagianopoulos, N.; Pappalardo, G.; Tsikoudi, I.; Amiridis, V. Validation of the TROPOMI/S5P aerosol layer height using EARLINET lidars. *Atmos. Chem. Phys.* **2023**, *23*, 1919–1940. [CrossRef]
43. Torres, O.; Jethva, H.; Ahn, C.; Jaross, G.; Loyola, D.G. TROPOMI aerosol products: Evaluation and observations of synoptic scale carbonaceous aerosol plumes during 2018–2020. *Atmos. Meas. Tech. Discus.* **2020**, *2020*, 6789–6806. [CrossRef]
44. Muñoz-Sabater, J.; Dutra, E.; Agustí-Panareda, A.; Albergel, C.; Arduini, G.; Balsamo, G.; Boussetta, S.; Choulga, M.; Harrigan, S.; Hersbach, H. ERA5-Land: A state-of-the-art global reanalysis dataset for land applications. *Earth Syst. Sci. Data* **2021**, *13*, 4349–4383. [CrossRef]
45. Li, C.; Dai, Z.; Liu, X.; Wu, P. Transport pathways and potential source region contributions of $PM_{2.5}$ in Weifang: Seasonal variations. *Appl. Sci.* **2020**, *10*, 2835. [CrossRef]
46. Rolph, G.; Stein, A.; Stunder, B. Real-time environmental applications and display system: READY. *Environ. Modell. Softw.* **2017**, *95*, 210–228. [CrossRef]
47. Sun, J.; Zhong, G.; Huang, K.; Dong, J. Banzhaf random forests: Cooperative game theory based random forests with consistency. *Neural Netw.* **2018**, *106*, 20–29. [CrossRef] [PubMed]
48. Chen, S.; Liang, Z.; Webster, R.; Zhang, G.; Zhou, Y.; Teng, H.; Hu, B.; Arrouays, D.; Shi, Z. A high-resolution map of soil pH in China made by hybrid modelling of sparse soil data and environmental covariates and its implications for pollution. *Sci. Total Environ.* **2019**, *655*, 273–283. [CrossRef] [PubMed]
49. Wang, J.; Ding, J.; Abulimiti, A.; Cai, L. Quantitative estimation of soil salinity by means of different modeling methods and visible-near infrared (VIS–NIR) spectroscopy, Ebinur Lake Wetland, Northwest China. *PeerJ* **2018**, *6*, e4703. [CrossRef]
50. Hong, Y.; Chen, S.; Liu, Y.; Zhang, Y.; Yu, L.; Chen, Y.; Liu, Y.; Cheng, H.; Liu, Y. Combination of fractional order derivative and memory-based learning algorithm to improve the estimation accuracy of soil organic matter by visible and near-infrared spectroscopy. *Catena* **2019**, *174*, 104–116. [CrossRef]

51. Liu, Y.; Zhu, Q.; Wang, R.; Xiao, K.; Cha, P. Distribution, source and transport of the aerosols over Central Asia. *Atmos. Environ.* **2019**, *210*, 120–131. [CrossRef]
52. Zhou, C.; Gui, H.; Hu, J.; Ke, H.; Wang, Y.; Zhang, X. Detection of new dust sources in central/east asia and their impact on simulations of a severe sand and dust storm. *J. Geophys. Res. Atmos.* **2019**, *124*, 10232–10247. [CrossRef]